Microtechnology Department

Head: Gábor Battistig, Ph.D.

Research Staff

G. **Battistig**, Ph.D.
I. **Bársony**, Ds.C.
Cs.S. **Daróczi**, dr. univ.
L.**Dózsa**, Ph.D.
P. **Fürjes**, Ph.D.
Z.J. **Horváth**, Ph.D.
Z. **Lábadi**, Ph.D.
G. **Molnár**, Ph.D.
A.E. **Pap**, Ph.D.
V. **Rakovics**, Ph.D.
G. **Vásárhelyi**, Ph.D.
Z. **Zolnai**, Ph.D.

M. **Ádám**, M.Sc. (part time)
F. **Beleznay** Ds.C. Prof. Emeritus
A. **Karacs**, M.Sc. (part time)
T. **Mohácsy**, M.Sc. (part time)
G. **Pető**, Ds.C. Prof. Emeritus
I. **Pintér** , Ph.D. (part time)
B. **Szentpáli**, Ph.D.
É. **Vázsonyi**, M.Sc. (part time)
Á. **Nemcsics**, Ph.D. (part time)
B. **Pődör,** Ph.D. (part time)

Vo Van **Tuyen**, Ph.D., (on leave)

Ph.D. students / Diploma workers

P. **Basa**, Ph.D. student
Á. **Németh**, Ph.D. student
Zs. **Baji** Ph.D. student
A. **Pongrácz**, Ph.D. student
K. **Gillemot** Diploma worker

Technical Staff

E. **Badalján**, engineer
Á. **Debreczeny**, engineer
J. **Ferencz**, engineer
Cs. **Lázár**, engineer
Á. **Majoros**, engineer
S. **Püspöki**, dr. techn. engineer (part time)
Zs. **Püspöki**, engineer
I. **Réti**, engineer
I. **Szabó**, dr. univ. engineer (part time)
T. **Szabó**, engineer
Á. **Szendrey**, engineer
J. **Waizinger**, engineer
K. **Veresné Vörös**, engineer
T. **Jászi**, engineer (on leave)

G. **Altmann**, technician
G. **Bíró**, technician
S. **Csarnai**, technician
M. **Erős**, technician
Cs. **Faragó**, technician
A. **Gondos**, technician
G. **Lehel**, technician
A. **Nagy**, technician
M. **Payer**, technician
M. **Varga**, technician

R. **Hodován**, diploma worker

T. **Berkó**, engineer (left)
V. **Kulin**, engineer (left)

The Microtechnology Department of MFA operates a 300 m^2 clean lab (Class 100-10000) with a complete Si-CMOS technology together with a mask shop. Another large facility of the Department is the CIGS solar cell laboratory equipped with a pilot line of a sputtering, an evaporation and a laser scribing module connected together with a sophisticated conveyor line for 30×30 cm^2 glass substrates.

The main tasks of the laboratory:

Research and development of physical, chemical/biochemical sensors and integrated systems:
- MEMS and MEMS related technology, with special emphasis on development of Si CMOS driving and readout circuitry.
- Development and applications of well tuned near IR light emitting diodes and detectors.
- Solar cells and their novel technology.
- Acoustic wave devices and their application.

Fundamental research on:
- novel sensing principles,
- novel materials and nanostructures,
- novel 3D fabrication techniques,
- and ion-solid interaction for supporting MEMS development are performed.

Device and material characterization:
- Various ion beam analysis methods.
- IR and Raman scattering.
- Scanning Microprobes.
- SEM, TEM, EDX, XRD.
- Spectroscopic Ellipsometry.
- Electrical characterisations.

The infrastructure of the clean lab is further developed in 2008, a new closed loop water cooling system has been installed. In order to increase the technical capabilities of the lab and to introduce new technologies (nanoimprinting, wafer bonding) into the MEMS developments, new equipments were purchased (Figures 1, 2, 3 and 4):

- SÜSS MicroTec MA 6 Manual Mask aligner for 3” and 4” wafers (4” and 5” masks)
    - manual loading
    - 0.7 μm precision
    - back side alignment
    - alignment toolset for wafer bonding
    - toolset for UV cured nanoimprint technology

- SÜSS MicroTec CB6L high vacuum anodic bonder
  - offering flexibility and accuracy for production and/or laboratory wafer
  - anodic bonding of two Si wafers of Si wafer to glass substrate,
  - aligned bonding of two or more wafers,
  - Supports thermo-compression bonding
  - with user friendly software allowing unlimited variations of process
  - bonding of aligned substrates up to 150mm in diameter.

To increase the quality of photolithography:

- Brewer Science Cee Model 200CB Spin Bake Unit
  - automated and programmable spin coater (0-12000 rpm)
  - programmable hotplate (<400°C)

- Brewer Science Cee Model 200 Spray Developer
  - for automatic and programmable developing of exposed photoresist.

In the next pages brief descriptions of the different tasks running in the lab are given. Some are not mentioned here because patenting processes of new sensing principles, technologies and devices are going on.

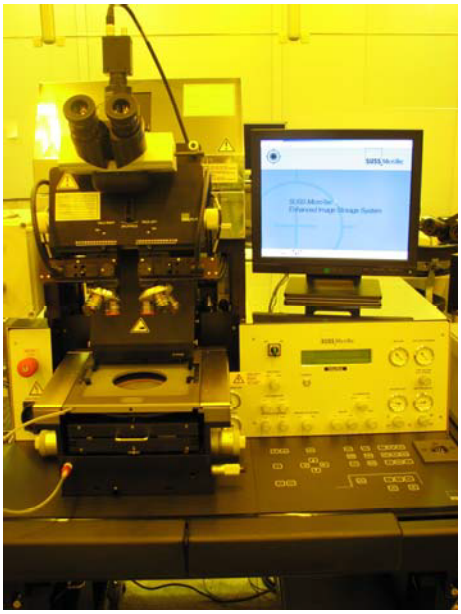

Figure 1 *SÜSS MicroTec MA 6 Manual Mask aligner with nanoimprint toolset*

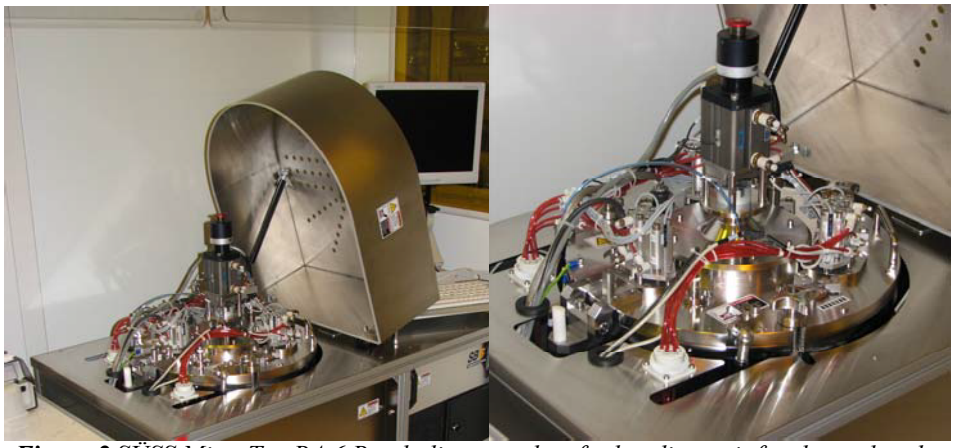

Figure 2 *SÜSS MicroTec BA 6 Bond aligner and wafer bonding unit for thermal and anodic bonding*

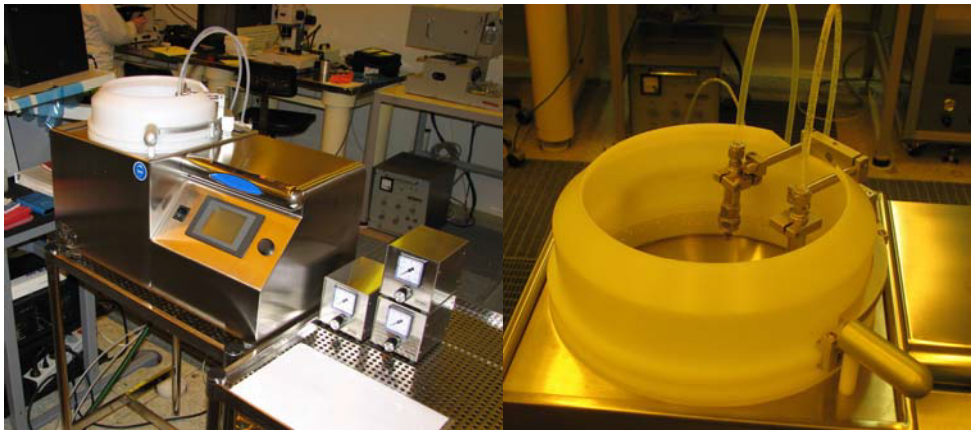

Figure 3 *Brewer Science Cee Model 200 Spray Developer for automatic and programmable developing of exposed photoresist*

Figure 4 *Brewer Science Cee Model 200CB Spin Bake Unit, automated and programmable spin coater and hotplate for photoresist*

Chemically Modified Solid-State Nanopores for Sensing

(Supported by Hungarian Scientific Fund (OTKA) NF69262)

P. Fürjes, A. L. Tóth, R.E. Gyurcsányi

Sensing with chemically-modified nanopores is an emerging field that is expected to have major impact on bioanalysis and fundamental understanding of nanoscale chemical interactions down to the single-molecule level. The main strength of nanopore sensing is that it implies the prospect of label-free single-molecule detection by taking advantage of the built-in transport-modulation-based amplification mechanism. At present, fabrication and application of solid-state nanopores are becoming to the focus of attention because, compared with their biological counterparts, they offer greater flexibility in terms of shape, size, and surface properties, as well as superior robustness.

We have reported on the fabrication of single channel solid-state nanopores fabricated by Focused Ion Beam etching, as well as on their chemical functionalization for selective detection of proteins and nucleic acids. Figure 1 represents the realisation method of solid-state nanopore combining the silicon bulk micromachining technology and nanoscale fabrication by FIB. The nanopores were etched in a free-standing silicon-nitride / gold layer structure manufactured by 3D MEMS technology.

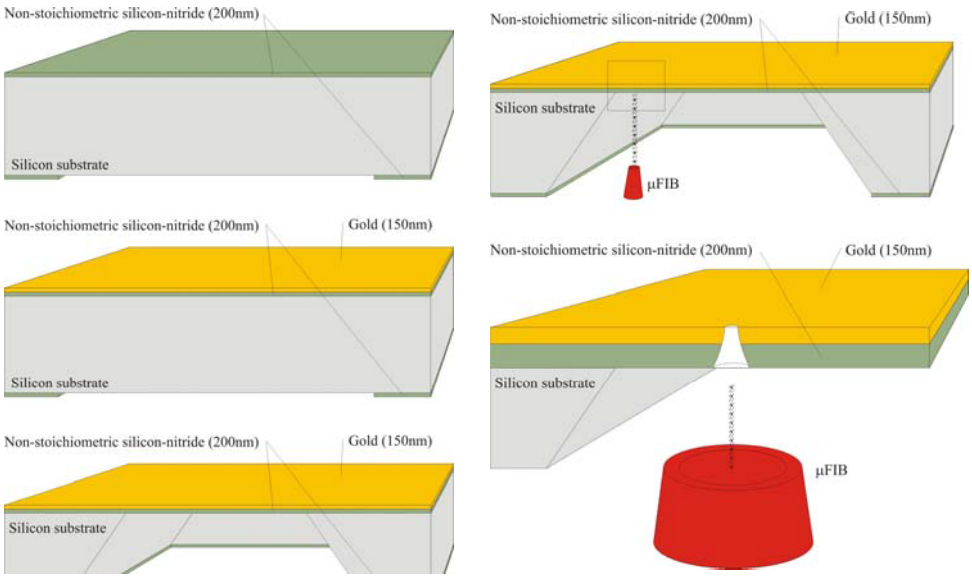

Figure 1 *Schematic representation of the fabrication process of the solid-state single nanopore by FIB*

The functionalisation of the nanochannels (Figure 2) passing through the gold layer and the method of transport-modulation-based selective molecule detection were developed by the Research Group for Technical Analytical Chemistry of the Hungarian Academy of Sciences at Budapest University of Technology and Economics. The transport-modulation based detection utilize the amplification mechanism i.e. species entering in the nanopore are acting on the electrical field or concentration induced flux of marker species (mostly, small ions provided by an electrolyte solution). In addition, to the label-free determination of target species, new hyphenated methods are introduced for signal amplification.

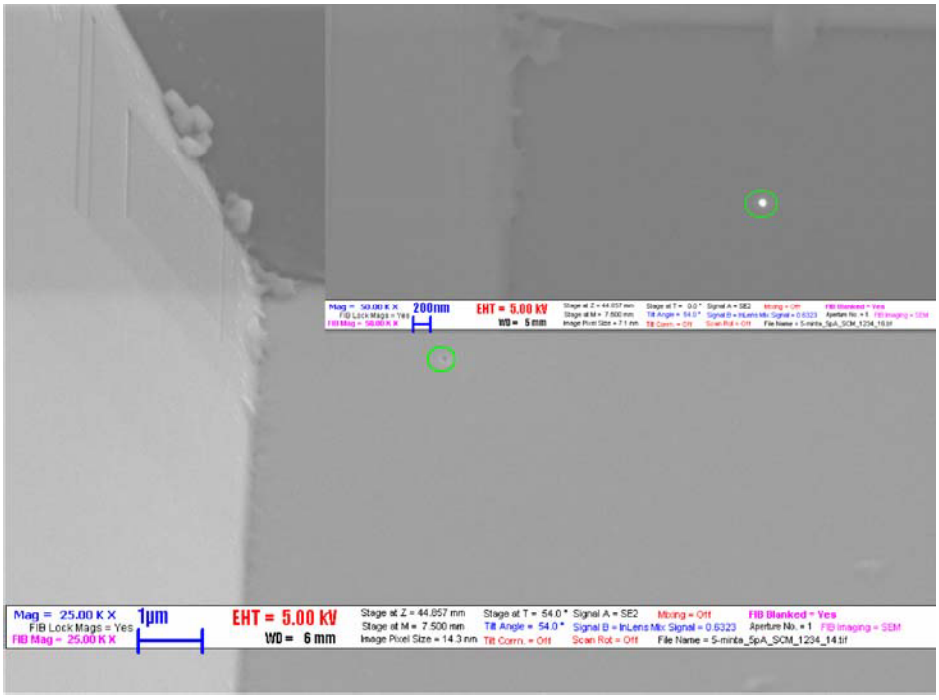

Figure 2 *SEM view of the single nanopore etched by FIB via the SiN_x / Au membrane (magnified in the inset))*

The capabilities of nanopore based sensors in terms of detection limit are explored by using random walk simulation and multiphysics modelling. Apparently, the detection limit of single nanopore based affinity sensor is determined by the probability of a successful encounter between the nanosensor and the solution. Since a single molecule can be in principle detected by nanopore sensors the limit of detection of such sensors has also explored in terms of concentration. However, significant improvements are obtained upon directing the solution by means of an electrical field or pressure gradient into the sensing zone of the nanopore.

Investigation of Actuation Phenomena and Controllable Moving Microstructures for Microfluidic Application

(Supported by Hungarian Scientific Fund (OTKA) F61583)

P. Fürjes

Realisation and application of controllable moving microstructures are the milestones of development microfluidic systems. The integrated microfluidic elements are essential components of lab-on-a-chip devices consisting of various elements: opened or embedded channels and cavities, fluid mixers and reactors. Smart devices are built up with additional active elements, typically heaters, sensors of various type and valves containing moving components for injection or facilitating the fluid flow in the required direction or in the reactor micro-vessel. To establish the research and development of complex microfluidic systems the investigation of actuation possibilities is essential.

The practicability of the actuation phenomena (electrostatic, magnetic and thermal) and the predictable functional parameters of the designed structures (deformation, driving frequency, residual stresses of the layer structures) were analysed by Finite Element Modelling. Test structures were manufactured by development and application the adequate MEMS techniques and analysed considering the functional aspects. The thermal actuation phenomena were analysed by realisation and investigation of a microfluidic valve system presented by Figure 1. The active part of the 3D MEMS structure were manufactured by silicon bulk micromachining applying platinum microheaters embedded in CVD deposited layer structure. The microchannels were formed by porous silicon micromachining and PDMS formation. Figure 2 shows the manufactured valve structure.

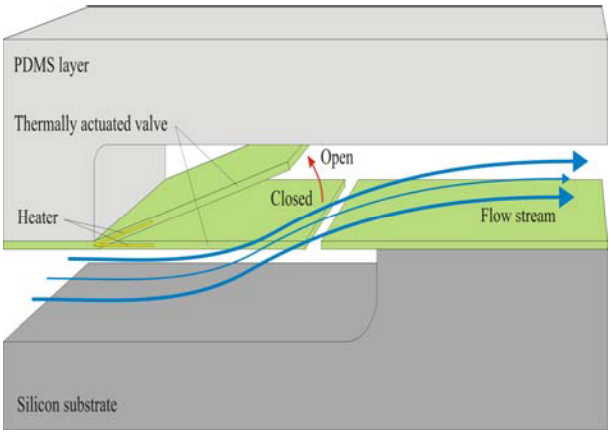

Figure 1 *Schematic representation of a thermally actuated microfluidic valve. The microfluidic channels are realized by the combination of 3D silicon micromachining and PDMS formation.*

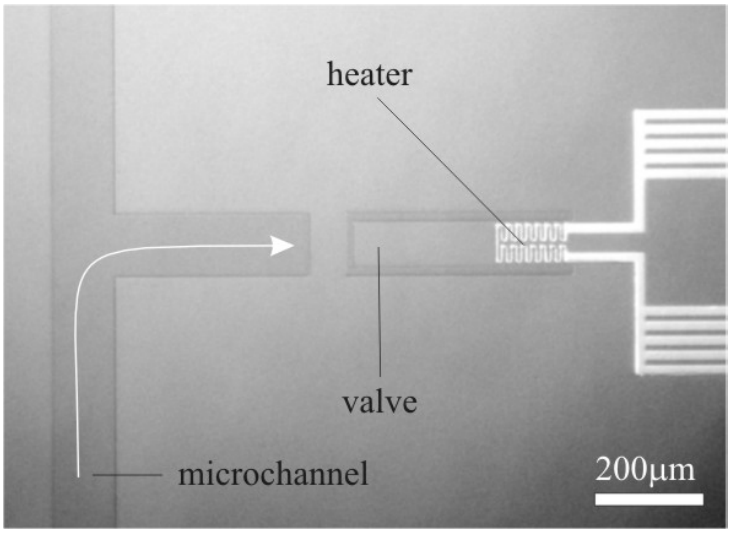

Figure 2 *Micrograph of the realized microfluidic system consisting valves*

Micro-heaters are basic components of sensors and lab on a chip devices, e.g. as sensors of calorimetric principle, or heaters in chemical micro-reactors. The most frequently used structural materials are silicon-nitride, non-stoichiometric silicon-nitride, silicon-oxinitride, silicon-dioxide and multilayered combination of these materials.

In the micro-heater design the most important parameters to be considered are the thermal conductivity, the thermal capacitance, linear expansion and the residual stress in the applied layers in order to select the optimum functionality of the device. While appropriate data are available for the widely used materials (SiO_2, Si_3N_4) this is far not being the case for the non-stoichiometric materials or deposited poly-crystalline silicon, diamond and DLC layers. Their properties are process dependent, i.e. both their composition and structure are determined by the given individual process. Therefore, relatively simple methods for determination of thermo-mechanical properties are essential in functional design. These thermo-mechanical properties were extensively analysed for proper prognostication of the functional parameters and behaviour of the active elements of the microstructures.

Si Micro-turbine by Proton Beam Writing and Porous Silicon Micromachining

(Supported by Hungarian Scientific Fund (OTKA) T047002)

P. Fürjes, Cs. Dücső, Z. Fekete, I. Rajta (ATOMKI, Debrecen)

Lab-on-a-chip MEMS are fabricated by various techniques: hot embossing, pressure moulding, laser ablation, LIGA or thick layer processing. Devices with complex functions are preferably formed from Si or combination of Si and other materials. The alternative key technologies are the alkaline etching of the bulk Si or the surface micromachining technique where the actuated membrane is formed from deposited polycrystalline Si or metal layers. The most promising technique for the formation of crystalline silicon components is the DRIE (Deep Reactive Ion Etching).

In the last few years proton beam writing in combination with porous silicon processing has been proposed for formation of high aspect ratio fixed 3D Si structures. Our group indicated that membranes of high displacement can also be fabricated by this technique. In the present work conventional microtechnology processes (thin layer deposition of non-stoichiometric silicon-nitride, polycrystalline Si and Al, double side photolithography, dry and wet etching techniques) are combined with PBW and porous Si micromachining for the fabrication of a silicon micro-turbine (Figure 1).

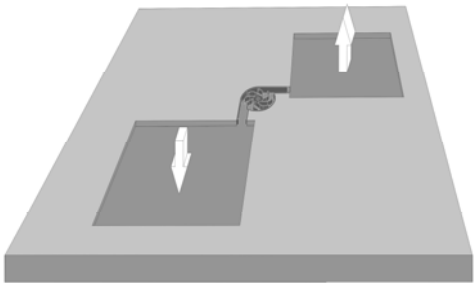

Figure 1 *The structure of the micro-turbine Si chip*

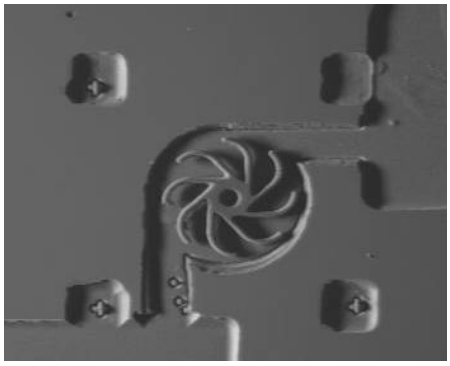

Figure 2 *SEM view of the processed micro-turbine chip*

A 3D Si micro-turbine (Figure 2) characterized by high aspect ratio vertical walls was formed by the combination of proton beam writing (PBW) and subsequent selective porous Si (PS) etching. Crystal damages generated by the implanted protons result in increased resistivity, thereby limit or even prevent the current to flow through the implanted area during electrochemical etching. Characteristic feature of the proposed process is that the shape of the micro electro-mechanical (MEMS) components is defined by two implantation energies. A higher energy is applied for defining the

housing of the device while the lower energy is used to write the moving components. The electrochemical etching is driven until the sacrificial PS layer completely underetches the moving components, but the etch-front does not reach the bottom of the housing.

This work is the first demonstration of a silicon device containing a moving part made by proton beam writing. The operation of the encapsulated device fabricated is successfully demonstrated (Figure 3-4).

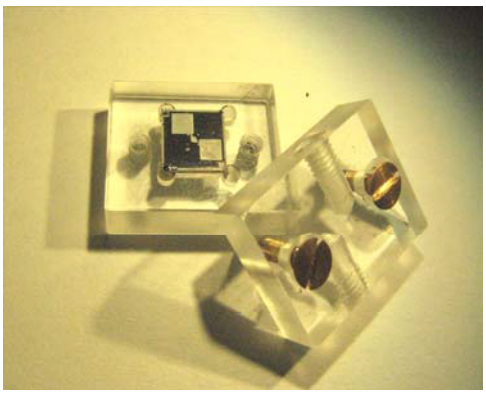

Figure 3 *Plastic housing of the micro-turbine chip*

Figure 4 *The rotating micro-turbine (see http://www.atomki.hu/atomki/VdG/ibaweb/video/)*

The aligned, two-energy proton beam implantation can provide high aspect ratio, completely or partially released microelements embedded in a cavity or a channel, thereby enabling us to form mobile components in the microfluidic MEMS.

Preliminary research for integrated Photo-acoustic Gas Detector System

(Supported by National Research and Development Programme NKFP3-00021/2005)

P. Fürjes, Z. Bozóki (Univ. Szeged)

An extremely sensitive photo-acoustic gas detector system is developed for analysis the methane and ammonia circulation of living forests. This method is based on the detection of the pressure wave generated by the selective energy absorption of the interested gas component excited by adequate laser-pulse in the test chamber. Beyond development of a micro cantilever microphone capable to detect the interested gas presenting in ppm range through the deformation of the suspended reflective micro-membranes, the applicability of an integrable microscale excitation source was considered.

3D MEMS structures including two optical microphones (Figure 1) were designed, developed and manufactured by double-side bulk micromachining silicon technology, fitting these structures to the active and reference flow chambers of the optoacoustic measuring system. The circumspect geometric and material design of the suspending multilayer microstructures is a crucial object of the research.

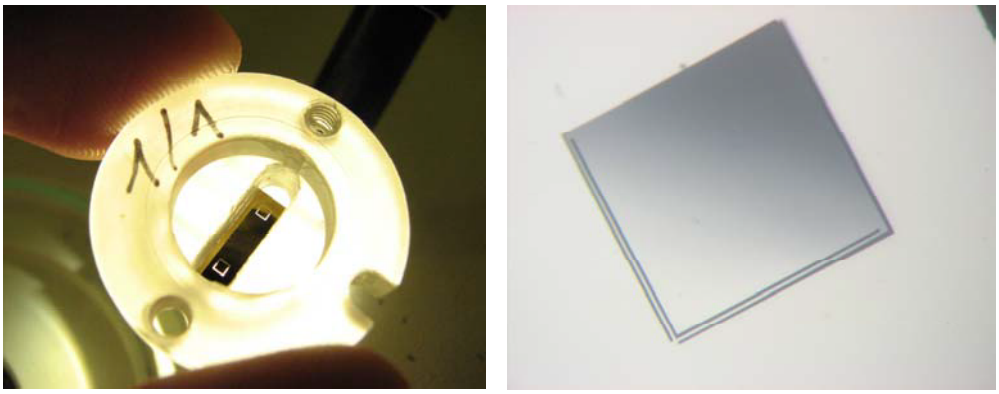

Figure 1 *Optical microphone structure (left) consisting cantilever membranes (right)*

Development and reliable realisation of a micro-scale excitation source is crucial for integration and miniaturisation of the photo-acoustic chamber and detection system. Adequate radiation spectra, integrability, long term stability, reliable operation are the basic requirements which have to meet the functional behaviour of the microheater structure. The special technology developed previously at MFA MEMS Laboratory for realisation microheater structures has completely improved (Figure 2). The manufactured suspended 3D micro-scale source (Figure 3) can fulfil the strict requirements of decreased power dissipation (reaching the temperature of 600°C at 20mW) due to the enhanced thermal insulation achieved by porous silicon sacrificial technology.

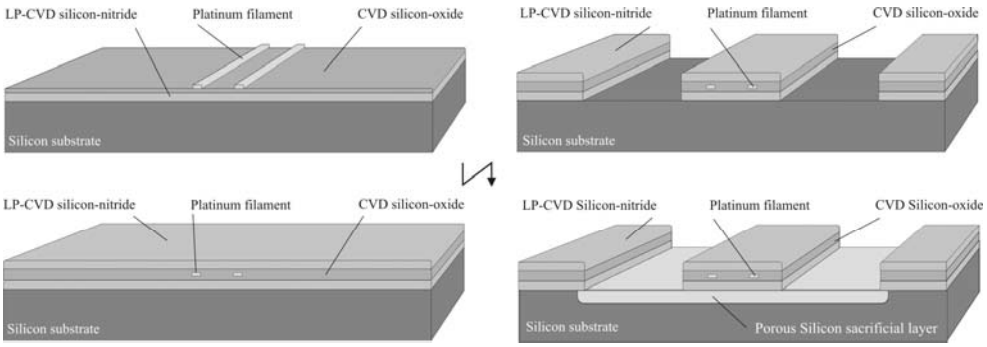

Figure 2 *Fabrication process of the integrable multi-layer microheater*

The adequate structural materials have selected by applying sophisticated finite element modelling for decreasing residual thermo-mechanical stress, and deformation as presented in Figure 4. The formerly applied simple non-stochiometric silicon-nitride suspension was improved by a symmetrical stacked layer structure consisting additional silicon-oxide layers decreasing deformation and mechanical instability of the source.

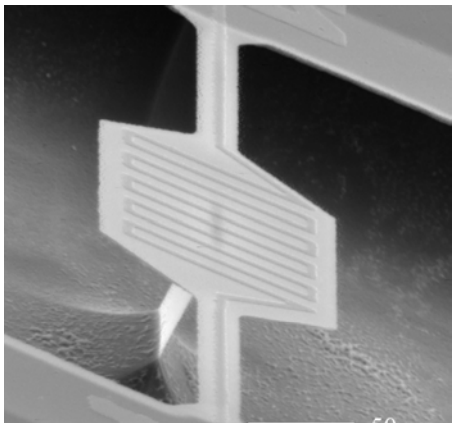

Figure 3 *Suspended structure applied as excitation source of photo-acoustic system*

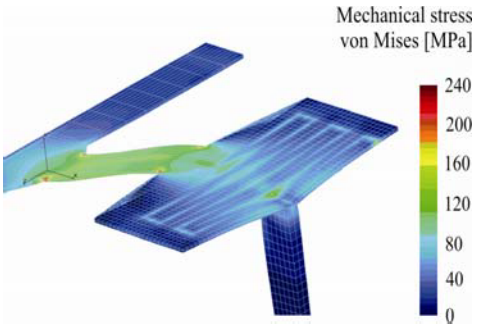

Figure 4 *Thermo-mechanical stress distribution of the heated structure*

Beyond the frequently applied structural materials, protective coating of MEMS elements used in harsh environment is essential for their reliable operation. The best candidates for such application are diamond, diamond-like-carbon (DLC) or SiC because of their superior chemical and abrasion resistance in aggressive chemicals. Applying a unique technique developed in corporation with BUTE a special micro-heater was manufactured replacing the structural materials by micro- and ultrananocrystalline diamond deposited by SAD (Selective Area Deposition) PE-CVD technique.

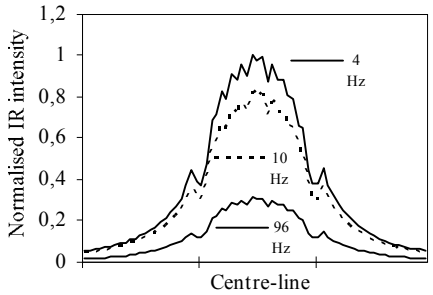

Figure 5 *IR intensity distribution along the centre-line of the source as the function of the driver frequency*

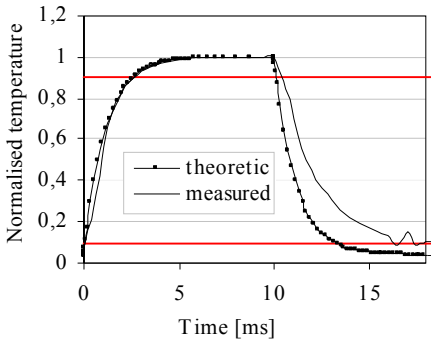

Figure 6 *Transient response of the heater driven by 10ms square wave excitation*

To ensure functional applicability of the micro radiation source the emissivity behaviour of the coating layers were investigated. The emission spectra of the source was analysed by using different top coating layers as doped poly-crystalline and amorphous silicon deposited by LP and PE CVD techniques, respectively.

The low power dissipation, high operating temperature and excellent transient behaviour are the significant requirements for the applicability of integrated micro sources. The transient response of the microstructure was tested by lock-in thermograpy recording the lateral distribution of the IR intensity using different driver frequencies. Figure 5 presents the frequency dependence of the radiated intensity distribution. The time response (Figure 6) of the structure was also analysed, the time constant of the thermal system was calculated for 1.1ms, and the frequency limit of the operation is several 10Hz.

Formation of SiC Nanocrystals in Si Based Systems by Reactive Annealing

A. Pongrácz, G. Battistig, D. Beke

Epitaxial formation of SiC nanocrystals on single crystal silicon surfaces by a simple and cheap reactive annealing in CO has been discovered and patented by BME AFT and MTA MFA. We have investigated the CO diffusion and SiC nanocrystal formation on different silicon based systems after 100% CO treatment at elevated temperatures (T>1000°C).

In cooperation with Institut des NanoSciences de Paris, SAFIR SiC nanocrystal formation was investigated by X-ray Photoelectron Spectroscopy at SOLEIL synchrotron. We identified the nc-SiC peak in the Si 2p XPS spectra. SiC was grown by heat treating single crystal silicon with 2.5 nm chemical oxide in 100% CO at 1100°C for 90 min at atmospheric pressure. Si-C binding energy was found at 100.56-100.61 eV after flashing off the oxide and the water vapor related contaminations. Fig. 1. shows the Si 2p peak deconvolution (Si-OH, Si-C, Si 2p ½, Si 2p 3/2 and surface states from left to right).

A continuous polycrystalline SiC layer formation as protective coating can have a great interest in harsh environment MEMS applications. Polycrystalline silicon unlike epitaxial Si can be deposited on arbitrary substrates and does not need exposed silicon underneath. Its good thermal stability, good interface to silicon dioxide, good conformality and ease of deposition and processing have made it a mainstay of silicon microelectronics technology. Single crystal silicon, polycrystalline silicon with 300 nm grain size and polycrystalline silicon with 100 nm grain size were used as a base structure for SiC growth in CO annealing. The comparison of the three samples after 3 hr CO heat treatment at 1100^{o}C is shown on Fig 2-4.

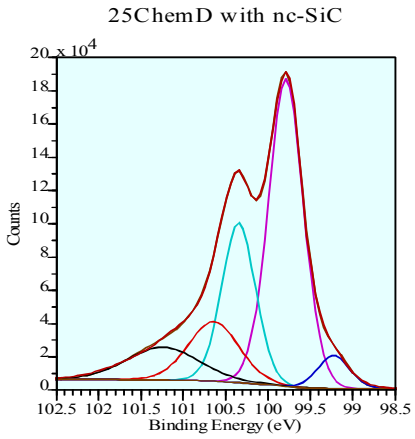

Figure 1 *Si 2p XPS peak from a single crystal Si surface covered with SiC nanocrystals*

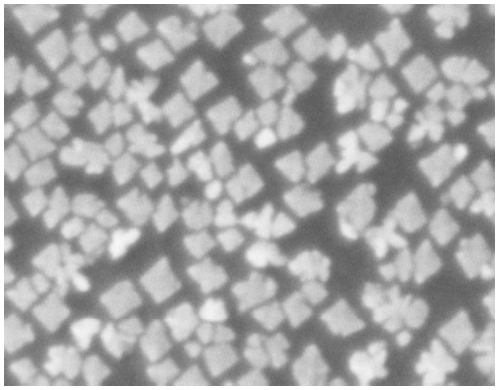

Figure 2 *SEM image of SiC nanocrystals on single crystal Si surface after oxide removal. Samples were heat treated in CO for 3 hrs at 1100°C.*

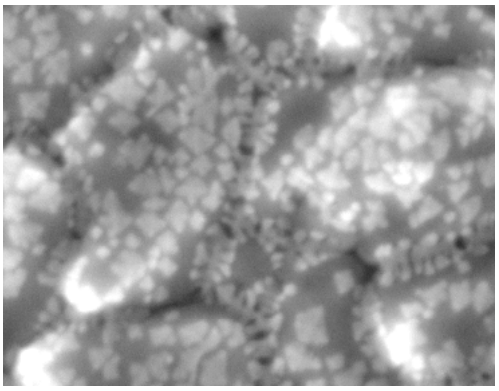

Figure 3 *SEM image of SiC nanocrystals on poly Si surface after oxide removal. Average grain size of poly-Si was 300 nm. Samples were heat treated in CO for 3 hrs at 1100°C.*

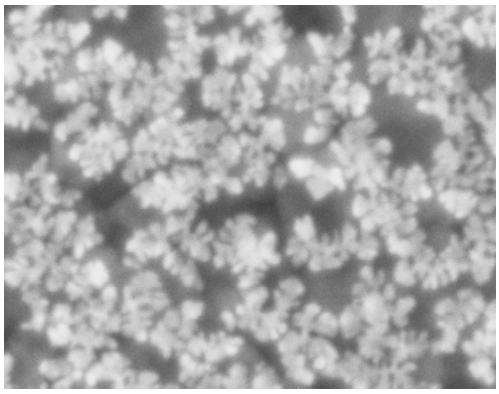

Figure 4 *SEM image of SiC nanocrystals on poly Si surface after oxide removal. Average grain size of poly-Si was 100 nm. Samples were heat treated in CO for 3 hrs at 1100°C.*

While on single crystal silicon the average grain size is 32 nm, on 300nm poly-Si the average SiC crystal size is 25 nm and on 100 nm poly-Si the typical SiC grain size is 20 nm.

SiC nucleation on poly-Si takes place on two characteristic areas: nucleation on the grain area and nucleation on grain boundaries. Nucleation density can be calculated on the grain area on 300nm poly-Si sample. Nucleation density is in the same range on the grain area as compared to the single crystal sample; however the growth rate is smaller. Nucleation at grain boundaries became the dominant phenomena as the grain

size is decreasing. On 100 nm poly Si sample nucleation on the grain area is almost never happen, while nucleation on grain boundaries shows a very high nucleation density and dendrite like crystal growth.

Semiconductor Nanocrystals in Dielectrics

(Supported by Hungarian Scientific Fund (OTKA) T048696)

Zs. J. Horváth, P. Basa

Semiconductor nanocrystals (NCs) are widely studied for non-volatile memory purposes. During this year our activity in this field was devoted to study $Si/SiO_2/Si_3N_4/Si$ NC/Si_3N_4 structures.

Three different samples were prepared. The first sample (GSR) was a reference structure without NCs. In the second one Si NCs were deposited for 60 s (SK) onto the thin Si_3N_4 layer. For the third sample (SN) Si NCs were deposited for 120 s onto the Si_3N_4 layer, but they were oxidized after deposition by the same HNO_3 treatment, as the tunnel oxide was prepared. After these steps the samples were covered with a 35 nm thick Si_3N_4 control layer. The cross-section of samples SK and SN are shown in Fig. 1.

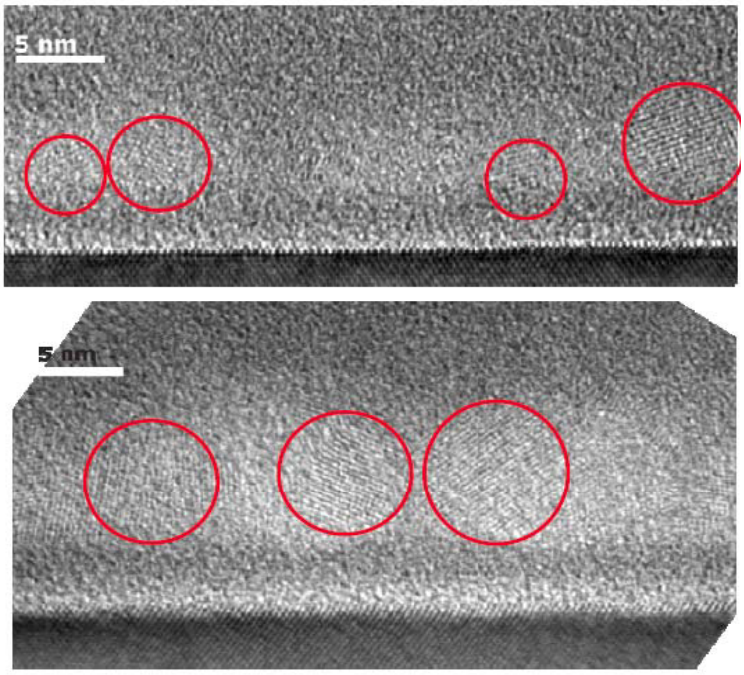

Figure 1 *High resolution transmission electron microscope images of two* $Si/SiO_2/Si_3N_4/Si$ *NC/*Si_3N_4 *structures*

Extremly good injection properties were obtained for samples SK and SN containing Si NCs, as presented in Fig. 2: the memory window width was about 3 V for charging pulses of ±6 V, 10 ms, and 15 V for pulses ±15 V, 10 ms. But the retention time was

very poor, a few seconds only. Nevertheless, due to the extremly good charge injection properties, similar structures can be good candidates for DRAM applications.

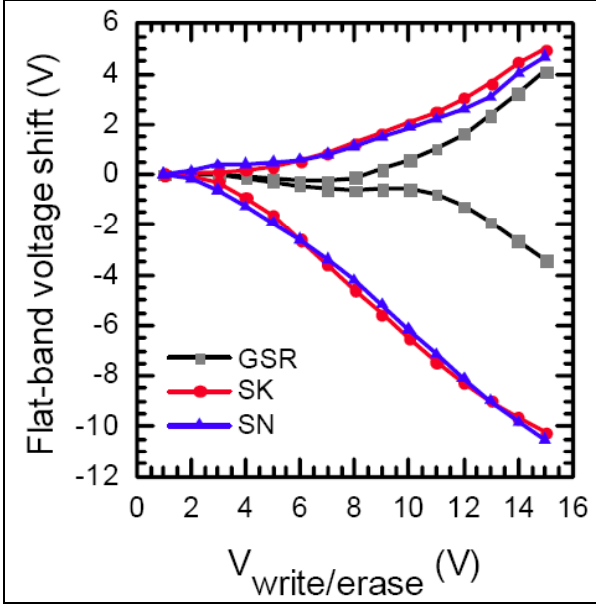

Figure 2 *The memory window of the two Si/SiO_2/Si_3N_4/Si NC/Si_3N_4 strucures referred in Fig. 1 (SK and SN. The memory window of the reference structure without Si NCs is also shown (GSR).*

Table 1. *The Ge nanocrystal deposition duration, the initial memory window width, its extrapolated values for 1 and 10 years, and the retention time for the studied SiO_2/Si_3N_4/Ge NC/Si_3N_4 structures for writing/erasing voltage pulses of ±15 V, 10 ms.*

Sample No.	NC deposition duration (s)	Initial memory window width (V)	Memory window width after 1 year (V)	Memory window width after 10 years (V)	Retention time (years)
G000	0	7.43	1.17	0.55	77.07
G025	60	7.93	1.88	1.35	3947.98
G050	120	7.68	0.86	0.22	21.64

Similar to the SiO_2/Si_3N_4/Si NC/Si_3N_4 structures, SiO_2/Si_3N_4/Ge NC/Si_3N_4 structures containig Ge nanocrystals were also prepared. In this case the duration of Ge NC depositon was studied as well (25 s and 50 s - samples G025 and G050, respectively). Opposite to the results obtained for similar structures with Si NCs, the Ge NC deposition improved the charging behaviour insignificantly, but the retention behaviour were very good (see Table 1). SiO_2/Si_3N_4/Ge NC/Si_3N_4 structures with Ge NC depostion duration of 25 s exhibited the best extrapolated retention time of about 4000 years.

Functionalization of Medical Implant Surfaces by High Energy Laser Pulses

(Supported by National Research and Development Programme NKFP 3/A 058-04/2004)

G. Pető, A. Karacs, G. Molnár

Although "Development and Application of Functionalized Surfaces in Specific Biochemical and Chemical System" Project, has formally ended in 2007, we continued this work for developing optimal human implant surface structures by laser assisted surface modification. The investigation of Ti surface structures has attracted interest because of can be applied as a material of medical implants, due to its excellent mechanical properties and its native oxide that is the reason of its biocompatible properties. The aim of this work was to modify the Ti surface in order to turn it into bioactive besides its biocompatibility. Pulsed laser surface treatment was used to achieve the desired bioactive properties. The resulted surface morphology of Ti implants depends on the energy and incidence angle of the laser pulses and on the pressure of the surrounding gases. Formation of different surface morphologies falling in the size range of 10 and 30 micrometer (Fig. 1(a)) may enhance the bonding between the implant material and the cells. Moreover, size of the proteins that are adsorbed on the surface typically falls into the nanometre size range (10-30 nm) (Fig. 1(b)) therefore a roughness with such a characteristic length can influence the process positively. On this way, bioactive behaviour was achieved, which results in faster and stronger osseo integration in medical practice.

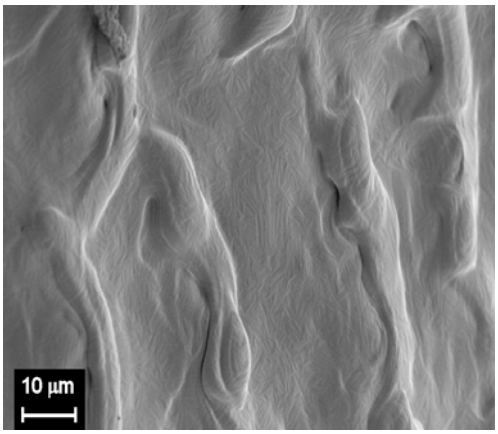

Figure 1(a) *SEM image of periodic micron-size waves on the surface of a screw shaped Ti implant after Nd:YAG pulsed laser treatment*

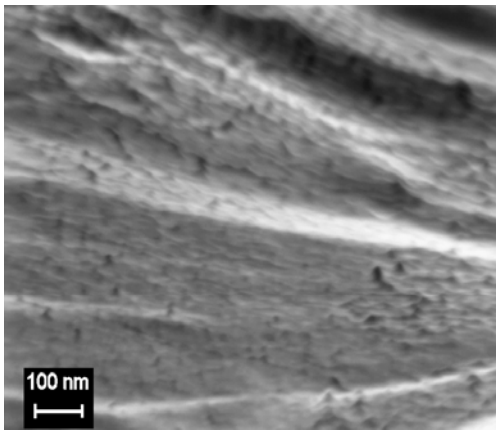

Figure 1(b) *SEM image of nano-sized morphology on the surface of a screw shaped Ti implant after Nd:YAG pulsed laser treatment*

Tactile sensor development and applications

TactoLogic Ltd.

G. Vásárhelyi

2008 was a successful year regarding tactile research and development at MFA. Through supports from our freshly founded spin-off, TactoLogic Ltd, we could continue our long-standing tactile sensor development with many different projects.

Our porous Si based piezoresistive MEMS technology has already stood the test of time through our general 4-element tactile arrays, capable of measuring 3D surface forces. These sensors have already been integrated into commercialized general tactile sensor products (TactoPad 2×2 and TactoFlex 2×2) through TactoLogic Ltd., and proved to be successful among the first users. In 2008 we also enhanced our measurement setup and techniques for high quality standardization of our sensors. We constructed a new measurement setup for precisely determining the functional properties (temperature dependence, multi-component response, linearity etc.) of our sensors.

Other development directions include the fabrication of 64 element integrated tactile arrays, where we combine MEMS and CMOS processes through a novel and unique patented technology. The first prototypes of the 8×8 type chips have been developed, the product integration processes are still running.

The last main development trend of the year is the construction of a single element miniature 3D tactile sensor, which is suitable for catheter applications mainly in the medical field. TactoLogic also realizes products based on this sensor, under the name TactoPoint 1×1.

TactoLogic Ltd. has started its evolution in 2007 and after one year of functioning could already realize profit from the commercialization of tactile sensors, which is an outstanding result among spin-off companies. Partly because of this, partly due to the great potential it holds, TactoLogic Ltd. has won this year's "Best spin-off/start-up Award" from the Hungarian Spin-off and Start-up Association, with the sponsorship of Ernst and Young.

Our future development trends include the integration of other modalities (e.g. temperature, humidity) into tactile sensing, the exploitation of viscoelastic properties of the elastic cover of the tactile sensors for bio-inspired and neuromorphic product development, and the construction of novel application-specific prototypes based on the current well-known technology.

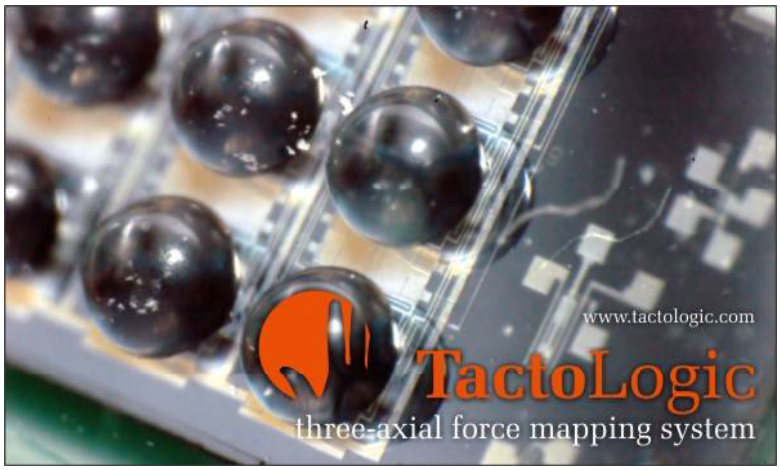

Figure 1 *Details of a 8×8 tactile sensor array with elastic covering plastic hemispheres (and TactoLogic Ltd's logo).*

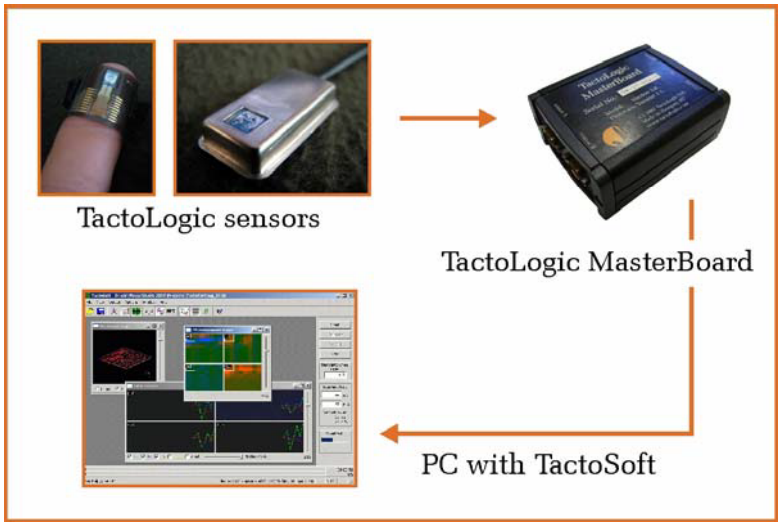

Figure 2 *Tactile development system based on MFA's 3D tactile sensors*

Tactile Sensor Development in the Microtechnology Lab in 2008 was mainly supported by TactoLogic Ltd., a spin-off founded in 2007 partly by MFA, with the mission of tactile R&D and commercialization. Throughout this year we developed and qualified several new tactile sensor prototypes for a wide range of commercial applications.

Increased Sensitivity Measurement of Point Defects by DLTS

L. Dózsa, G. Molnár, J. Ferencz, and S. Lanyi

The detection and identification of contamination in silicon is of technological importance. We have investigated microscopic, structural, and electric properties if FeSi2 layers. [Vouroutzis N, et al., Journal of Alloys and Compounds 448 (2008) 202, Tsormpatzoglou A, et al., J. Appl. Phys 100 (2006) 0733139]. Scanning probe capacitance microscope (SCM) was found to give information on silicon surface contamination [Dózsa L, ET AL., Appl. Surf. Sci. 234 (2004) 60]. For understanding the electrical properties, measurements with high spatial resolution are needed. The modern devices of few micron size require measuring apparatus of increased sensitivity.

In this work we suggest a method of point defect identification. The corresponding electrical characteristics are measured by the conventional DLTS system but with using a preamplifier.

The method is illustrated by measurement of Fe contaminated silicon. $FeSi_2$ quantum dots were grown on n-type (100) silicon. In the Fe deposited layer a resistive layer with high concentration of Fe related defects dominate the characteristics. The concentration of the Fe related deep level defects outside the Fe deposited region is comparable to the shallow dopant concentration near the silicon surface as it is shown in Figure 1 by a series of frequency scan DLTS spectra of a large area Schottky junctions. The defect is attributed to Fe contamination.. Capacitance-voltage characteristics and capacitance DLTS frequency scan of the measuring tip positioned at 5 micron distance from the silicon surface is shown in Fig.2. Both the C-V and DLTS characteristics are equivalent to them measured in macroscopic Schottky junctions. By measuring small junctions the preamplifier increases the sensitivity capacitance 200 times, while the current sensitivity increases 1000 times, which enables measurement of junctions of small area. The realization of the surface scale requires nanopositioning of the preamplifier and the measuring tip in the DLTS cryostat.

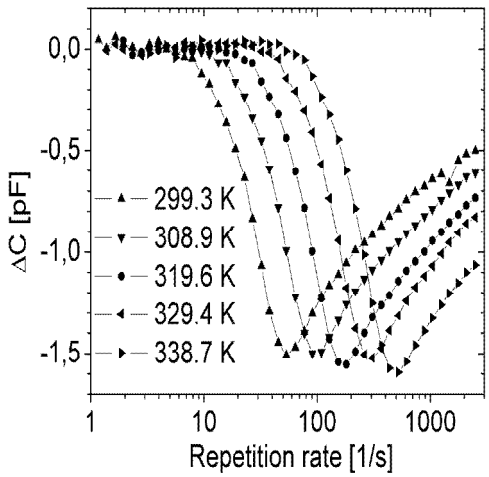

Figure 1 *DLTS frequency scan spectra measured in DLS-83D system at 299.3 K, 308.9 K, 319.6 K, 329.4 K, and 338.7 K temperatures.*

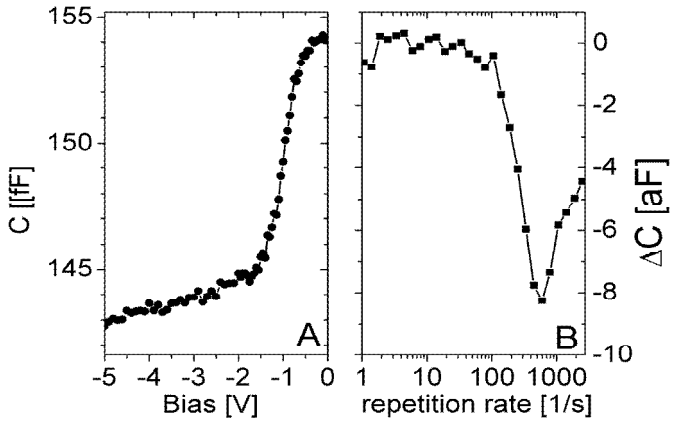

Figure 2 *C-V characteristics (A) and DLTS frequency scan (B) measured by the capacitance preamplifier with a 50 μm diameter tip positioned at 5 μm distance from the free silicon surface*

Si Surface Preparation and Passivation by Heavy Water Vapour

A.E. Pap, G. Battistig

Due to the shrinking feature size, the characteristics of the interface under the gate dielectrics play a crucial role in the performance of MOS devices; therefore, interface engineering is a key issue in processing. In cooperation with Mattson Technology, Inc. we investigated the stability of the H and D passivated Si surfaces against native oxidation in normal air.

We demonstrated that deuterium adsorbs on Si surface at room temperature much stronger than hydrogen. Moreover, in case of deuterium passivated wafers the vacuum storage can be omitted without risking the non–controlled native oxidation of silicon for up to 5 hours or more. It could be a suitable and more robust surface cleaning and passivation process for the industry, but heavy water is expensive. As a cheaper procedure, we presented that 1 min vapour phase treatment at 65 ºC of heavy-water (D_2O) + 50% HF (e.g. 20:1) mixture was enough to remove the native oxide and to passivate the Si surface without any degradation of the atomic surface flatness. The surface evolution of the D-passivated surface was followed by contact angle measurements, by spectroscopic ellipsometry (SE), by atomic force microscopy (AFM), by X-ray photoelectron spectroscopy (XPS), by transmission electron microscopy (TEM) and by infrared absorption spectroscopy (IR) qualification and the results were compared to the H-passivated Si surface.

Combination of D passivation with rapid thermal process (RTP) based on the thermal desorption kinetics of the adsorbed D and/or H layers on Si is a promising method for improved interface engineering and for better initial reactions in case of ultra thin dielectric layer formations. In order to confirm this statement we created Si_xN_y thin layer on D (Fig. 1.) and H passivated Si surface by using RTP. The typical Schottky-like current-voltage characteristics obtained on the studied Al/SiN_x/n-Si structures are. Both H and D treatments influenced the I-V behaviour much, but in opposite way: H treatment yielded lower current through the structure, while D treatment resulted in much higher current level, than that obtained for the untreated structure. In addition, the shape of the forward branch of the I-V curves (Fig. 2.) changed and its slope became more abrupt after both H and D treatments. The results indicate that the current flow through the structures is limited by the conductance trough the SiN_x layer and by the potential barrier at the Si surface. The parallel shift of the curves along the current (vertical) axis is due to the effect of H and D treatment on the density of interface states at the SiN_x/Si interface, while the change of the shape and slope is probably connected with the effect of treatments on the conductivity of the SiN_x layer. Taking into account the Al and Si work function difference, the charge in interface states increased after H treatment, while it decreased significantly after D treatment indicating an affective passivation of Si surface.

These results confirmed that using D passivation on Si surface is a promising method in the MOS technology and the interface engineering processes.

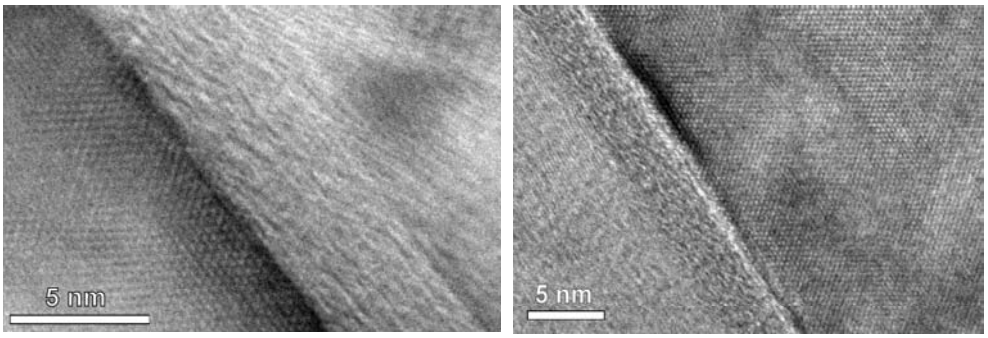

Figure 1 *Oxy-nitride layer thickness on (a) H-passivated wafer 4.35 nm and on (b) D-passivated 3.5 nm.*

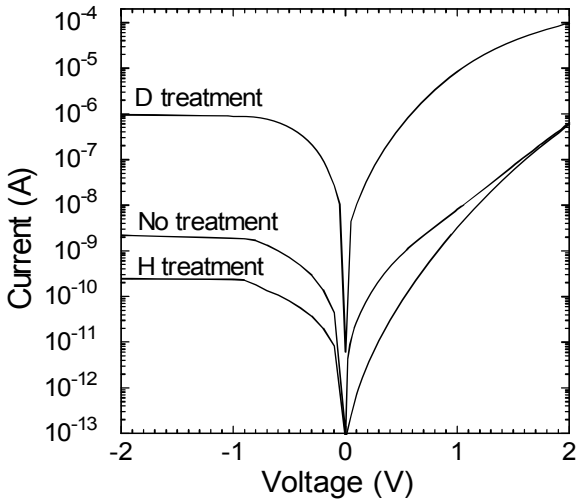

Figure 2 *Typical current-voltage characteristics of the studied Al/SiN_x/n-Si structures.*

The Effect of Ion Irradiation on Ordered Colloidal Nanoparticulate Masks

Z. Zolnai, A. Deák, N. Nagy and A.L. Tóth

In nanotechnology, fabrication represents the first and one of the most significant challenges to the realization of nanostructures. A promising method to create arrays of small objects on a substrate is nanosphere lithography (NSL) which was pioneered in the early 1980's [Fischer U C et al, J. Vac. Sci. Technol. 19 (1981) 881] and was further developed by several groups. In NSL, a self-organized layer of colloidal spheres is used as a mask for a lithographic step such as illumination, ion implantation, deposition, or etching. When NSL is used for masking, an array of nanostructures, arranged in closely packed hexagonal symmetry, is left on the substrate surface (deposition) or embedded in the substrate (implantation). NSL is a simple, fast, and inexpensive method to create large arrays of nanostructures.

The Langmuir-Blodgett (LB) technique is commonly used to prepare molecular films from Stöber silica nanospheres. Fig. 1(a) shows a monolayer LB film of ∅ 450 nm Stöber silica nanospheres deposited on (100) Si substrate.

As recent studies show, ion implantation through a LB nanomask leads to the deformation of the mask due to ion-nanoparticle interactions. The nature and the intensity of the deformation process strongly depend on the size of the nanospheres and the implantation parameters (ion energy, mass, and fluence). One of the most striking example of the shaping effect is the deformation of single colloidal particles under MeV energy irradiation with heavier ions [T van Dillen et al, Appl. Phys. Lett. 78 (2001) 910]. In this case spherical silica colloids expand perpendicular to the ion beam and contract parallel to the ion beam changing their shape to oblate ellipsoidal. This phenomenon – called „ion hammering" – is due to the fact that amorphous materials subject to high-energy ion irradiation can undergo anisotropic plastic deformation [Klaumunzer S et al, Phys. Rev. Lett. 51 (1983) 1987]. With the different applications evolving and for fundamental understanding it becomes important to find the key parameters that determine the deformation rate. As our preliminary experiment showed, already at 0.5 MeV Xe^{2+} ion energy ion hammering occurs for ∅ 450 nm silica spheroids, see Fig. 1(b). In this case the average penetration depth (~220 nm) of the ions is comparable to the diameter of the spheres (i.e. both masking and deformation occurs) so that our experiment gives valuable information about the potential and limits of NSL.

Scaling down the diameter of the spheres one has to decrease the energy of the bombarding ions to satisfy the geometrical conditions for masking (selective area patterning). Even so, to date only a few attentions were paid to ion-nanomask interactions in the energy range of 10-100 keV. A recent study [Lindner J K N et al., Nucl. Instrum. Methods Phys. Res. B 242 (2006) 167-169] has shown that the irradiation of ∅ 100 nm silica spheres with 15-75 keV energy C^+ ions leads to different effect than ion hammering. In that case the collective motion and coalescence of the spheres was observed, an effect called „ion beam sintering". In our preliminary study

performed in a focused ion beam (FIB) setup with 30 keV Ga^+ ions we found significantly different behaviour of colloidal silica spheres for ∅ 450 nm than for ∅ 90 nm under similar irradiation conditions, see Fig. 1(c) and (d). For the larger spheres no collective motion and sintering is observed, instead the silica colloids contract perpendicular to the ion beam changing their shape to cylindrical like. For the smaller spheres ion beam sintering occurs.

The details and cause of the size effect and the sintering process are not yet completely understood, however, they play clearly fundamental role in the NSL technique. Our recent plan is to give significant contribution to this research area.

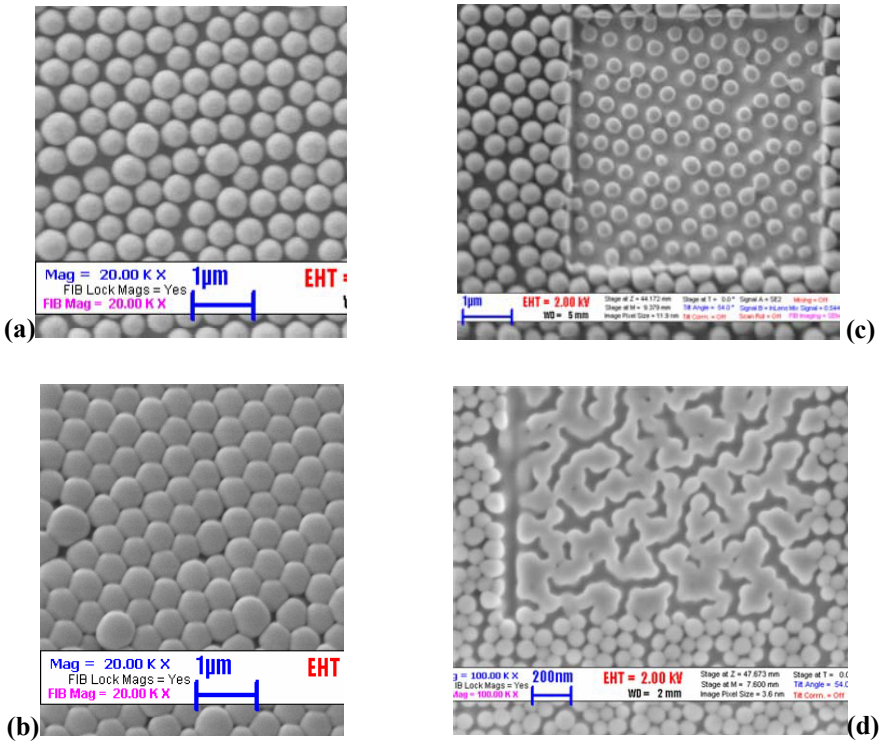

Figure 1 *(a) FESEM image of one monolayer Stöber silica spheres with diameter of 450 nm deposited on Si substrate using Langmuir-Blodgett (LB) technique (unirradiated film). (b) A similar film after irradiation with 500 keV Xe^{2+} ions: shape transformation from spheres to oblate ellipsoids occurs (anisotropic plastic deformation, or ion hammering effect). (c) A similar LB film irradiated with 30 keV Ga^+ ions: size reduction without collective motion of the spheres can be observed. (d) One monolayer of ∅ 90 nm Stöber silica nanospheres deposited on Si substrate irradiated with 30 keV Ga^+ ions: collective motion of the spheres and ion beam sintering can be observed.*

Orientation Dependence of the Thermal Relaxation of Damage in 4H-SiC Introduced by High Fluence Ni Implantation

Z. Zolnai, G. Battistig, A.L. Tóth, J. Garcia López, and Y. Morilla

Nowadays the investigation of single crystalline silicon carbide (SiC) is an intensive research area. The unique physical properties of SiC, especially the wide band gap, make it suitable for spintronics applications. One possibility to introduce magnetic ions (Fe, Co, Cr, Ni, Mn, etc.) with high concentration (ca. 0.1-10 atomic %) into SiC is ion implantation. This process results in the formation of lattice damage which leads to degradation and unstable operation of the devices. The problem to optimize the post-implantation annealing process in order to recover the damaged crystal lattice is not yet solved, however, one have to overcome this obstacle before SiC can be used in spintronics devices. It is an important issue to study the effect of annealing on SiC layers pre-amorphized with high fluence Fe^+, Mn^+, Ni^+, etc, implantation.

We investigated the thermal recovery of 860 keV Ni^+ implantation-induced damage on the surface and throughout the implanted layer in 4H-SiC. The results for two different crystalline orientations, namely the (0001) and (11-20) planes were compared, see Fig 1.

In the FESEM micrographs in Fig. 1, largely different changes in the surface morphology for (0001) and (11-20) orientations can be observed after post-implantation annealing at 1150 ^oC for 1 hour. In the former case a pattern of cracks with trigonal or hexagonal symmetry is formed on the 10 micron scale, while in the latter case parallel cracks appear with a spacing of about 10 micron. For higher magnification in Fig. 1 (b) wire-like structures can be observed by FESEM indicating the formation of a polycrystalline zone during annealing. For (11-20) orientation similar structures cannot be seen as the surface appears to be quite homogeneous. These results are in agreement with previous observations performed on Al^+ ion implanted SiC samples [Battistig G et al, J. Appl. Phys 100 093507 (2006)] showing that for (0001) orientation cubic (3C) polycrystalline inclusions appear after a similar annealing treatment. The recent results on Ni implanted samples show that for (11-20) orientation the hexagonal character – nevertheless, in the presence of planar defects – can be recovered.

The above described qualitative trends were confirmed with 3.5 MeV He^+ ion backscattering/channeling (BS/C) measurements (not presented here) which have shown that despite the high Ni atomic concentration of 0.5 %, i.e. the high implantation fluence (being ca. 20 times higher than the amorphization threshold for SiC), the long range ordered hexagonal character of the (11-20) oriented substrate is preserved throughout the whole 770 nm thick implanted layer after annealing.

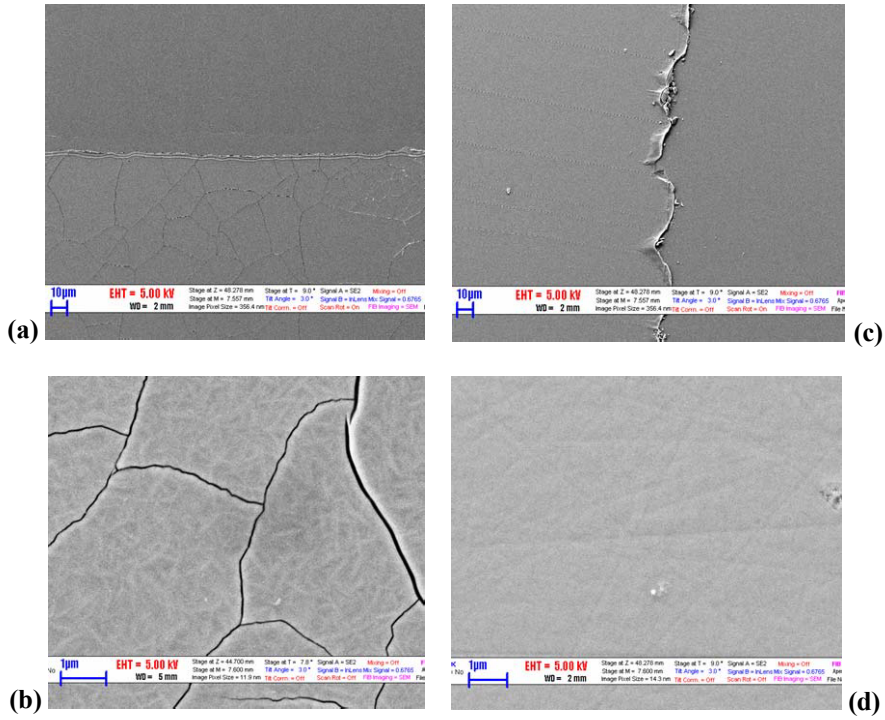

Figure 1 *The effect of post-implantation annealing on the surface morphology of (0001) and (11-20) oriented 4H-SiC samples irradiated with 860 keV Ni^{+} ions to a fluence of 1×10^{16} cm^{-2}. The annealing process was performed at a temperature of 1150 ^{o}C for 1 hour.*
To the top: FESEM micrographs taken at the border of the as-implanted and post-implantation annealed regions for (a) (0001) and (c) (11-20) oriented surfaces.
To the bottom: FESEM micrographs with higher magnification taken on the relaxed surfaces after the annealing treatment. (b) The wire-like structures with diameter of ~50 nm are well visible on the (0001) oriented surface, while (d) they are absent on the (11-20) oriented plane. Here only scratches, probably due to the original surface polishing, are visible.

Bandgap Engineering of Quaternary GaInAsP Semiconductor for Application as Active Layer in Optoelectronic Devices Used for Food Spectroscopy

V. Rakovics

Infrared emitting diodes play an important role in the development of portable spectrometers due to their high efficiency compared to conventional lamps. Quality control in food industry and clinical diagnostics demand powerful, versatile and relatively not expensive spectrometers. Semiconductor light sources are characterized by small dimensions and low power consumption. They can therefore be regarded as suitable components for low price miniature devices.

The GaInAsP/InP alloy system is widely used for fabricating optical devices, because GaInAsP can be epitaxially grown lattice matched on InP substrates over a wide range of band gaps from 1.34 eV (920 nm) to 0.74 eV (1680 nm) at room temperature.

Liquid phase epitaxy (LPE) were used for development of the device structures, as the composition of the active layer can be relatively easily adjust by weighing appropriate amount of the materials into the growing melts. By development of the precise experimental phase diagram, LPE growth of new GaInAsP device structures became fast and reliable fabrication method.

Near-infrared (NIR) spectroscopy is based on the absorption of electromagnetic radiation at wavelengths in the range 780–2500 nm. NIR spectra of foods comprise broad bands arising from overlapping absorptions corresponding mainly to overtones and combinations of vibrational modes involving C-H, O-H and N-H chemical bonds. The concentrations of constituents such as water, protein, fat and carbohydrate can in principle be determined using classical absorption spectroscopy. NIR spectroscopy is used routinely for the compositional, functional and sensory analysis of food ingredients, process intermediates and final products. The major advantage of NIR is that usually no sample preparation is necessary, hence the analysis is very simple and very fast (between 15 and 90 s) and can be carried out on-line. One of the strengths of NIR technology is that it allows several constituents to be measured concurrently. In addition, for each fundamental vibration there exists a corresponding series of overtone and combination bands with each successive overtone band approximately an order of magnitude less intense than the preceding one. This provides a built-in dilution series which allows several choices of absorptions of different intensity containing the same chemical information. Finally, the relatively weak absorption due to water enables high-moisture foods to be analyzed. NIR spectroscopy is well suited for determining the major components of foods such as water, fat, and protein. The reason why NIR spectroscopy is well suited when assessing the presence of water and protein is due to the specificity of O–H and N–H bindings. In the overtone region from 1000 to 1900 nm water can be observed around 1400–1550 nm, and this overlap to some extent with the N–H regions from 1490 to 1600 nm.

GaInAsP/InP is an ideal material system for the fabrication of double heterostructure devices. As InP has higher band gap than the lattice matched GaInAsP active layer, absorption losses inside the devices structure can be minimized. Additionally, waveguide layers, gratings, optical filters, can be grown from the same type of material. However light emitting diodes have narrow spectral bandwith compared to conventional lamps and in most applications a series of different wavelength devices is needed to cover the wavelength range of the analyzed components. For optimal overlapping of the LED array spectra not only the peak emission wavelengths but the spectral widths are equally important to be designed carefully. High quality GaInAsP LEDs have been developed for emission in the 900-1700 nm range and the emitting wavelength of these devices can be tuned by changing the composition of their active layers. Liquid phase epitaxy is a versatile tool for growing thick layers with various composition simply by weighing different amount of materials into the melts. LPE grown infrared emitting diodes have 50-75 meV spectral bandwidth depending on the growth conditions. Small area surface emitting LED chips were prepared to cover the 1000-1700 nm wavelength range completely. These chips were efficiently used for food spectroscopy. Fig 1 shows the infred photo of high brigthness LED chip. Figure 2 shows the relative near infrared transmission spectra of ethanol and water.

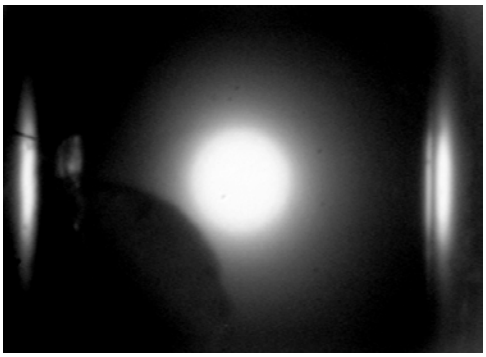

Figure 1 *Infrared photo of high brightness GaInAsP/InP IR-LED chip*

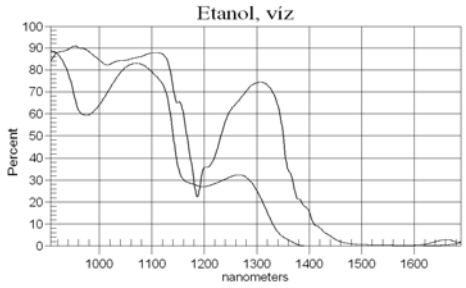

Figure 2 *NIR transmission spectra of ethanol and water*

In 2008 we have developed high brightness IR LED chips for selective spectroscopy of ethanol- water solutions and for photo-acoustic water vapour.

Co-evaporated Four-Component Semiconductor Thin Films for Photovoltaics - Solar Cell Innovation Center

(Supported by Hungarian National Research Fund (OTKA) Project NK 73424)

Z. Lábadi, Á. Németh, I. Bársony

Aim and achievements:

The aim of the Solar Cell Innovation Center is to develop an R&D facility for thin film solar cells with CuInGaSe active layer. The cross-section of the solar cell structure is shown in Fig. 1.

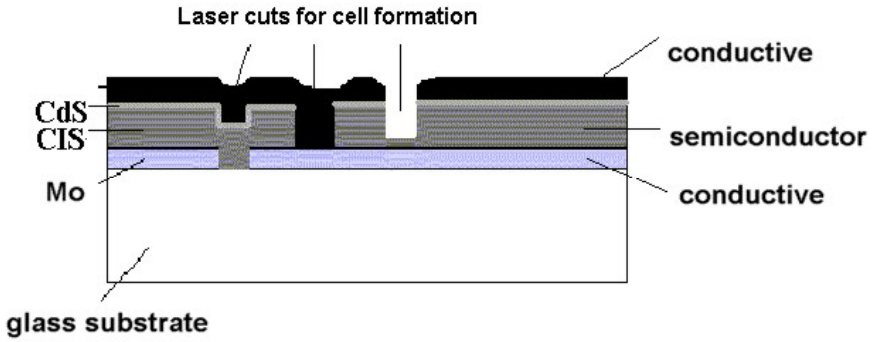

Figure 1 *Structure of CIGS solar cell*

1. Co-evaporated four-component semiconductor thin films for photovoltaics

The research project is aimed at the understanding of fundamental phenomena and the interrelation of composition, structure and optical / electrical properties vs. growth and deposition parameters in the active layer of CIGS PV devices.

The project is aimed to study the main materials related issues in p-type CIGS such as

- Shallow acceptor doping by intrinsic defects in CIGS
- Bandgap engineering in CIGS
- Grain boundary and grain-size
- Na-diffusion effect
- Bandgap matching by the buffer layer
- Buffer layer growth by Atomic Layer Deposition (ALD)

2. Results related to the reactive sputtering of Al doped ZnO contact layers

Reactive sputter deposited ZnO received much attention in the solar cell technology during the past few years due to its cost efficiency. The key issue for its introduction into mass production was the deep understanding of the reactive sputter process.

The most notable difficulty is the well known hysteresis effect of the reactive plasma just in the range of the system parameters necessary for excellent property Al:ZnO TCO thin films.

Detailed study of the deposited layers vs. deposition parameters made possible the identification of different regions in the power vs. oxygen flow chart of the system. These are summarized in Fig 2.

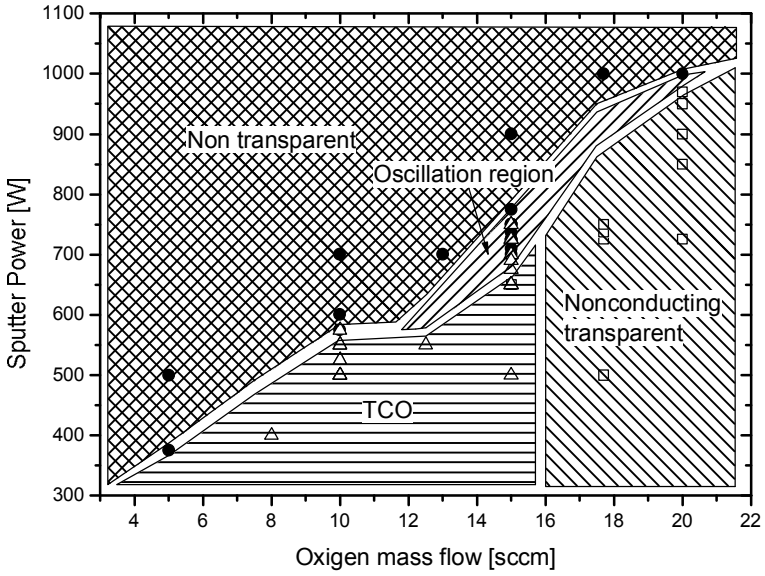

Figure 2 *Detailed study of TCO deposited layers vs. deposition parameters*

A. Metallic region ("non -transparent" in Fig 2.) showed inadequate transparency but high conductivity
B. Above 15sccm oxygen mass flow the layers were transparent but insulating as well. ("Nonconducting transparent" in Fig. 2.)
C. Spontaneous and stable plasma oscillations were observed in the oscillation region (See Fig. 2.). Fig. 3 shows the time dependence of the working pressure and the target voltage in this domain while Fig. 4 shows a cross-sectional TEM micrograph of a sample deposited from oscillating plasma. A qualitative physical model for the oscillation was also developed.

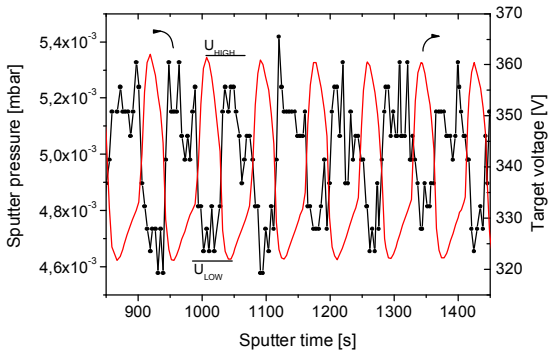

Figure 3 *Time dependence of the working pressure and the target voltage in the oscillation domain*

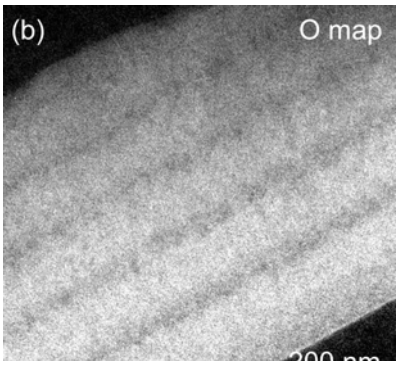

Figure 4 *TEM micrograph of a sample deposited from oscillating plasma.*

D. On the basis of our experimental findings reproducible deposition of TCO layer is possible at target power values below 750 W and at oxygen inlets less than 15 sccm ("TCO in Fig.2.") An optimal working point can be defined in the 550 - 575W power range and at 10/40sccm O/Ar gas flow where 7.7×10^{-4} Ωcm TCO layer with 90% transparency can be deposited without closed loop process control and substrate heating.